Chemical Physics Letters 832 (2023) 140885

Contents lists available at ScienceDirect

Chemical Physics Letters

journal homepage: www.elsevier.com/locate/cplett

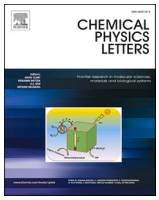

Kinetic study of C1 criegee intermediate with diethylamine and ethylamine and their atmospheric implications

Jiayu Shi [a,b], Haotian Jiang [b,c], Li Che [a,*], Siyue Liu [b,d], Yang Chen [b,e,f], Xueming Yang [b,g], Wenrui Dong [b,h,*]

[a] Department of Physics, School of Science, Dalian Maritime University, Dalian 116026, Liaoning, China
[b] State Key Laboratory of Molecular Reaction Dynamics, Dalian Institute of Chemical Physics, Chinese Academy of Sciences, Dalian 116023, China
[c] Department of Chemical Physics, School of Chemistry and Materials Science, University of Science and Technology of China, Hefei 230026, China
[d] Key Laboratory of Materials Modification by Laser, Ion, and Electron Beams, Chinese Ministry of Education, School of Physics, Dalian University of Technology, Dalian 116024, China
[e] Key Laboratory of Chemical Lasers, Dalian Institute of Chemical Physics, Chinese Academy of Sciences, Dalian 116023, China
[f] University of Chinese Academy of Sciences, Beijing 100049, China
[g] Department of Chemistry, Southern University of Science and Technology, Shenzhen, 518055, China
[h] Hefei National Laboratory, Hefei 230088, China

A B S T R A C T

This paper investigates the pressure and temperature-dependent kinetics of CH_2OO reacting with diethylamine (DEA) and ethylamine (EA) using the OH laser-induced fluorescence method. Pressure independence was observed within the range of 5.4–75 Torr. The rate coefficients for these reactions at 298 K are (2.49 ± 0.39) × 10^{-11} and (8.14 ± 1.25) × 10^{-12} cm^3 $molecule^{-1}$ s^{-1}. The activation energies, determined from experiments conducted between 283 and 328 K, are (−2.01 ± 0.08) and (−1.35 ± 0.02) kcal mol^{-1}. These reactions may contribute to the degradation of DEA and EA under specific environmental conditions.

1. Introduction

Ozone oxidation is a prominent pathway for the atmospheric consumption of alkenes [1]. This process involves the addition of ozone to the unsaturated double bond of alkenes, resulting in the formation of a primary ozonide (POZ) with a five-membered ring. Subsequently, the POZ undergoes rapid rearrangement and dissociation, leading to the generation of a carbonyl compound and a carbonyl oxide, commonly referred to as Criegee intermediates (CIs) [2,3]. These reactions are highly exothermic, releasing approximately 200–250 kJ mol^{-1} of energy. Consequently, a portion of this energy is transferred to the CIs, which exist in vibrational excited states denoted as CIs* [4,5]. Upon formation, some of the CIs* rapidly dissociate into products such as OH and CHO, while others are stabilized through collisions with bath gases, forming stable Criegee intermediates (SCIs) [6,7].

SCIs have a relatively long lifetime, allowing them to participate in bimolecular reactions with atmospheric trace gases [7–10]. These reactions have significant implications not only for tropospheric chemical pollution but also for environmental concerns such as aerosol formation, and the generation of acid rain [11,12]. Consequently, SCIs have a crucial impact on the atmospheric environment. Among the various processes involved in the fate of CH_2OO, the reactions between CH_2OO and water vapor, sulfur dioxide, and formic acid are primary pathways for the removal of CH_2OO in the atmosphere [13].

Ammonia and amines are important nitrogen-containing organic compounds found in the atmospheric environment. Among them, ammonia is the most abundant alkaline substance in the atmosphere. The atmospheric amine mass, take the measurement in the San Joaquin Valley of California for example, ranges from 14 to 23 % of ammonia mass, and EA and DEA accounted for 25–45 % of total amine mass [14]. These compounds originate from various sources, including both anthropogenic and natural origins. Anthropogenic sources include activities such as agricultural fertilization, animal husbandry, and wastewater treatment processes. Natural sources encompass emissions from plants and soils. Amines play an important role in new particle formation (NPF), thereby influencing the chemistry of atmospheric aerosols [15–18]. Notably, their nucleation-promoting abilities surpass that of ammonia [19,20]. In the marine atmosphere, Iodic acid (IA) has been recognized as an important driver for NPF, and Ma et al. found that DEA exhibits the highest potential among amines and O/S-atom-containing

* Corresponding authors at: State Key Laboratory of Molecular Reaction Dynamics, Dalian Institute of Chemical Physics, Chinese Academy of Sciences, Dalian 116023, China (Wenrui Dong).
E-mail addresses: liche@dlmu.edu.cn (L. Che), wrdong@dicp.ac.cn (W. Dong).

https://doi.org/10.1016/j.cplett.2023.140885
Received 17 August 2023; Received in revised form 30 September 2023; Accepted 11 October 2023
Available online 14 October 2023

acids in promoting the IA-induced nucleation [21].

The reaction between CH_2OO and ammonia has been extensively studied, with reported rate coefficients ranging from 5.64 to 8.4×10^{-14} cm^3 $molecule^{-1}$ s^{-1} at room temperature [8,22]. Combining experimental and theoretical approaches, Liu et al. [22] found that this reaction exhibits weak temperature dependence, and Chhantyal-Pun et al. [8] reported that the product of this reaction is a functionalized organic hydroperoxide adduct, formed through the insertion of CH_2OO into the N—H bond of ammonia.

Kumar et al. calculated that the barrier of reactions between SCIs (CH_2OO, *syn-/anti*-CH_3CHOO) and amine in the gas phase decreases with increasing methyl substitution on the amine [23]. Reactions of CH_2OO with methylamine [8] and *tert*-butylamine [24] are measured to be negative temperature dependence, and no obvious pressure dependence at 10–75 Torr, with the rate coefficient of $(5.6 \pm 0.4) \times 10^{-12}$ cm^3 $molecule^{-1}$ s^{-1} at 293 K for the former reaction and $(4.95 \pm 0.64) \times 10^{-12}$ cm^3 $molecule^{-1}$ s^{-1} at 298 K for the latter. Vansco et al. observed that the reaction of *syn-/anti*-CH_3CHOO with DMA generated the insertion product (amine-functionalized hydroperoxide), and their calculation indicated that the DMA reaction with *anti*-CH_3CHOO is faster than with *syn*-CH_3CHOO by up to 34,000 [25].

In this study, we investigate the kinetic of the reactions between the simplest Criegee intermediates, CH_2OO, and DEA and EA. We explore the pressure and temperature dependence of these reactions using the OH laser-induced fluorescence technique. The pressure range examined is 5.4–75 Torr, while the temperature range spans from 283 to 328 K. Based on the obtained rate coefficients, we have conducted an analysis to evaluate the atmospheric impact of these reactions on the depletion of DEA and EA.

2. Experimental method

The reaction kinetics of CH_2OO with DEA and EA were investigated by measuring the OH radical produced from the decomposition of CH_2OO using OH laser-induced fluorescence (OH LIF) method. The experimental setup (shown in Fig. S1) and procedures have been previously described in the literature and are summarized here [26–29].

The experiments were carried out in a quartz flow tube reactor. CH_2I_2 (TCI, ≥98 %) contained in a bubbling bottle was heated to a temperature of 35 °C using a water bath and was carried to the flow tube reactor by Ar. The concentration of CH_2I_2 was determined by measuring its ultraviolet absorption spectroscopy using deep ultraviolet lamp (DUV325-H46, Roithner Laserthchnik) and an adjustable gain photodetector (PDB450A, Thorlabs). $(C_2H_5)_2NH$ (0.1 % in Ar), $C_2H_5NH_2$ (0.1 % in Ar), O_2 (99.999 %), and balanced/carrier gas Ar (99.999 %)) were introduced independently and continuously into the flow tube reactor through separate mass flow controllers (MKS, GS50A Series). The total pressure inside the flow tube reactor was measured using a capacity manometer (MKS Baratron) and was actively controlled using a scroll dry vacuum pump (Edwards XDS46i) and an exhaust throttle valve (MKS 653B). The temperature of the flow tube reactor was regulated using a temperature-controlled circulator (Yin Der BL-730) and monitored using a K-type thermocouple (Omega, TECK25-9) positioned near the detection region.

The chemical reactions were initiated by photolyzing CH_2I_2 in the presence of O_2 using the third harmonic (355 nm) of a Nd:YAG laser (Beamtech, Nimma 900) with a beam diameter of 5 mm. The OH radicals were excited by the double frequency (282 nm) of the output of a dye laser (Narrow Scan High Rep, Rhodamine 590 dye, 2 mm diameter) pumped by a high repetition rate Nd:YAG solid-state laser (Edgewave INNOSLAB:IS12II-ET, 10 kHz). In the flow tube reactor, the photolysis laser and the detection laser intersected perpendicularly, and the time delay between the two lasers was controlled by a digital delay pulse generator (Stanford Research System, DG645).

The 282 nm laser excited OH through the P1(1) line of the (1,0) band of the OH ($A^2\Sigma^+ \leftarrow X^2\Pi$) transition. The OH fluorescence signal passed through a stack of optical filters (Schott UG11, Semrock FF02-320/40-25 and Semrock FF01-315/15-25), and was amplified by a photomultiplier tube (PMT, Electron PDM9111-CP-TTL), collected by a multichannel scaler (Ortec MCS-PCI), and recorded on the computer. To improve the signal-to-noise ratio, OH time-dependent profiles were accumulated over 1500 photolysis pulses.

3. Discussion

CH_2OO is generated from the following reactions:

$$CH_2I_2 + h\nu \rightarrow CH_2I + I \quad (R1)$$

$$CH_2I + O_2 \rightarrow CH_2IOO \quad (R2a)$$

$$\rightarrow CH_2OO + I \quad (R2b)$$

The consumption of CH_2OO is as follows:

$$CH_2OO \xrightarrow{k_{3a}} OH + HCO \quad (R3a)$$
$$\xrightarrow{k_{3b}} \text{other products} \quad (R3b) \quad (R3)$$

$$CH_2OO + (C_2H_5)_2NH \xrightarrow{k_{4a}} \text{Products} \quad (R4a)$$
$$CH_2OO + C_2H_5NH_2 \xrightarrow{k_{4b}} \text{Products} \quad (R4b) \quad (R4)$$

$$CH_2OO + X \xrightarrow{k_5} \text{Products} \quad (R5)$$

$$CH_2OO + CH_2OO \xrightarrow{k_6} \text{Products} \quad (R6)$$

OH consumption is described by the following reactions:

$$OH + Y \xrightarrow{k_7} \text{Products} \quad (R7)$$

The time-dependent OH (v '' = 0) signal can be described as follows (See our previous work for details) [26]:

$$S_{OH}(t) = \frac{A_0(k_3 + k'_4 + k'_5)}{(k_3 + k'_4 + k'_5)e^{(k_3+k'_4+k'_5)} + 2k_6[CH_2OO]_0(e^{(k_3+k'_4+k'_5)} - 1)} - A_1 e^{-k'_7 t} \quad (1)$$

where $A_0 = \gamma \frac{k_{3a}[CH_2OO]_0}{k'_7-(k_3+k'_4+k'_5)}$, $A_1 = \gamma \frac{k_{3a}[CH_2OO]_0}{k'_7-(k_3+k'_4+k'_5)} - [OH]_0$, γ is the detection efficiency for OH. $k'_4 = k_4[reactant]$, $k'_5 = k_5[X]$ and $k'_7 = k_7[Y]$. X denotes species that consume CH_2OO other than DEA and EA, including I, IO, CH_2I_2. Y represents species that consume OH, such as IO, CH_2I_2, DEA, and EA. $[CH_2OO]_0$ represents the initial concentration of CH_2OO, which is in the range of 4.43–5.21 × 10^{12} cm^{-3}. $[CH_2OO]_0$ was determined by the yield of CH_2OO from $CH_2I + O_2$ reaction [30], the concentration of CH_2I_2, the absorption cross section of CH_2I_2 [31], and the calculated flux of the photolysis laser (see the Supporting Information for detail). $[OH]_0$ represents the instant OH originated from the reaction of excited CH_2I^* with O_2 [29]. During fitting the OH time-depended profiles, parameters A_0, A_1, $k_3 + k'_4 + k'_5$, and k'_7 were floated, and k_6 was fixed to values reported by Ting et al [30].

Fig. 1 shows the OH time-dependent profiles for the reaction between CH_2OO and $(C_2H_5)_2NH$ at various concentration of $(C_2H_5)_2NH$. As the $(C_2H_5)_2NH$ concentration increases, the OH signal decays faster, indicating the reaction between CH_2OO and $(C_2H_5)_2NH$. The solid lines are the fits of experimental data with equation (1) using 1stOpt 7.0 software (7D-soft High Technology Inc). The values of $k_3 + k'_{4a} + k'_5$ could be obtained from the fits. Since $k_3 + k'_5$ are independent of $[(C_2H_5)_2NH]$, when plot $k_3 + k'_{4a} + k'_5$ against $[(C_2H_5)_2NH]$, the slope of the linear fit is k_4, and the intercept is $k_3 + k'_5$.

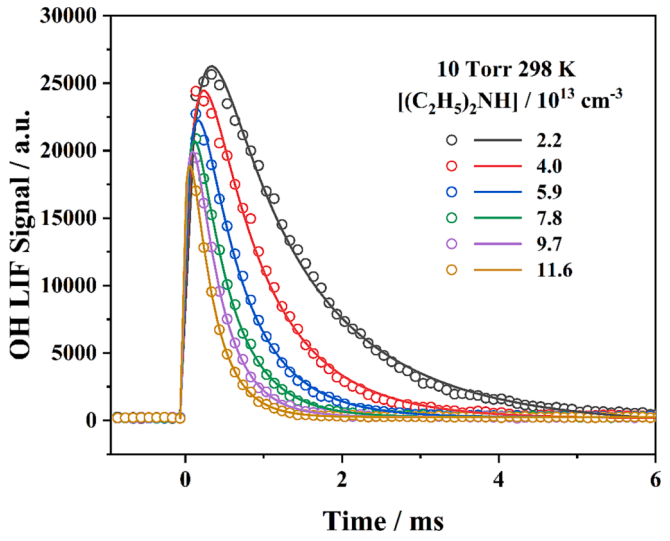

Fig. 1. OH time-dependent profiles in the presence of various $[(C_2H_5)_2NH]$ at 298 K and 10 Torr. The circled points are the experimental data, and the solid lines are the fits of experimental data with equation (1).

3.1. Pressure and temperature dependence

Fig. 2 shows the pseudo-first-order loss rate of CH_2OO as a function of $(C_2H_5)_2NH$ and $C_2H_5NH_2$ at 30 Torr and 298 K. These reactions were found to be independent of pressure within the range of 5–75 Torr, and the average values provide the best estimates of the rate coefficients: $(2.49 \pm 0.39) \times 10^{-11}$ and $(8.14 \pm 1.25) \times 10^{-12}$ cm^3 $molecule^{-1}$ s^{-1} at 298 K for the CH_2OO reactions with $(C_2H_5)_2NH$ and C_2H_5NH, respectively. Further details on the rate coefficients, along with the experimental conditions, can be found in Table S1 and S2 in the Supporting Information. The values from the fits were given in Tables S3 and S4 in the Supporting Information.

Fig. 3 shows the rate coefficients for CH_2OO reactions with $(C_2H_5)_2NH$ and $C_2H_5NH_2$ at 298 K and 5.4–75 Torr, respectively. The error bars in the figure represents the total error of rate coefficients (for more information, refer to the Supporting Information). The reactions between SCIs and ammonia/amines proceed through the insertion of SCIs into the N—H bond of ammonia/amines [32,33]. Kumar et al.

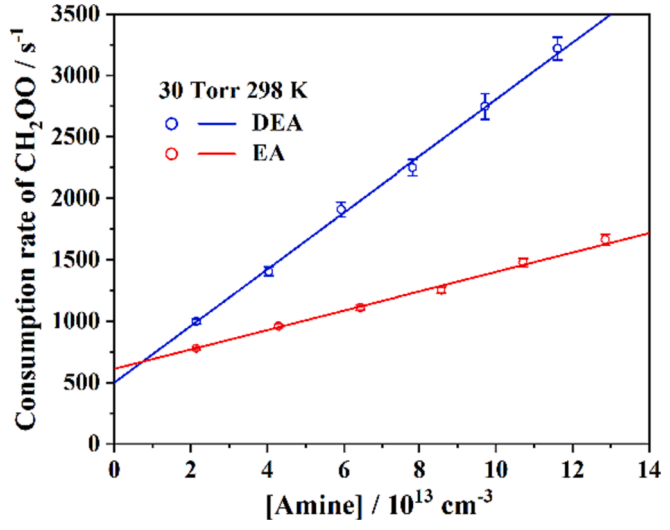

Fig. 2. Pseudo-first-order loss rate of CH_2OO at 30 Torr and 298 K. The error bar represents one standard deviation from fitting the OH time-dependent profiles.

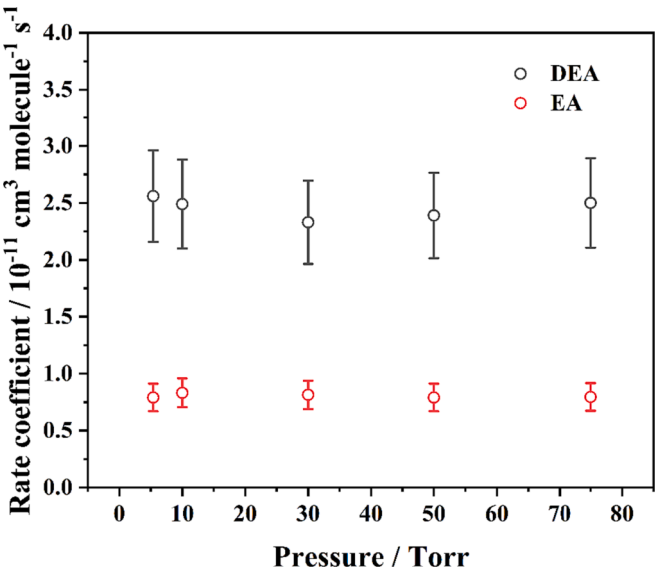

Fig. 3. Measured rate coefficients for CH_2OO reaction with $(C_2H_5)_2NH$ and $C_2H_5NH_2$ as a function of total pressure at 298 K. The error bar of each rate coefficient represents total experimental errors (15.7 % for CH_2OO reaction with DEA and 15.3 % for that with EA, for details, see the Supporting Information).

conducted high-level quantum chemical calculations and Born Oppenheimer Molecular Dynamics (BOMD) simulations, which suggested that the barriers for SCIs reacting with amines decrease with increasing methyl substitution on the amine, to the extent that the reaction between CH_2OO and $(CH_3)_2NH$ is barrierless [23]. It is highly likely that the title reactions are barrierless, with no extrema in the reaction pathway between the 1,2-insertion products and the reactants of CH_2OO with $(C_2H_5)_2NH$ and $C_2H_5NH_2$, which could explain the observed pressure independence in the current experiment.

Both reactions exhibit negative temperature dependence, as evidenced by the decreasing slopes with increasing of temperature, shown in the Fig. S2 in the Supporting Information. The average values of the bimolecular rate coefficients, k_{4a} and k_{4b}, obtained at different temperatures, are listed in the Table 1. For more detailed information, please refer to Tables S5 – S8 in the Supporting Information.

Fig. 4 presents the Arrhenius plot for the CH_2OO reaction with $(C_2H_5)_2NH$ and $C_2H_5NH_2$, with the error bars representing the total experimental error. The activation energy and pre-exponential factor derived for the CH_2OO reaction with $(C_2H_5)_2NH$ are (-2.01 ± 0.08) kcal mol^{-1} and $(8.16 \pm 1.16) \times 10^{-13}$ cm^3 $molecule^{-1}$ s^{-1}, respectively. Similarly, for the CH_2OO reaction with $(C_2H_5)_2NH$, the derived values are (-1.35 ± 0.02) kcal mol^{-1} for the activation energy and $(8.33 \pm 1.03) \times 10^{-13}$ cm^3 $molecule^{-1}$ s^{-1} for the pre-exponential factor.

The reactions involving amines, alcohols, H_2O, and NH_3 with SCIs proceed via 1,2 insertion reactions. Chhantyal-Pun et al. have proposed that the rate coefficients of 1,2 insertion reactions of CH_2OO are correlated to the labile hydrogen bond dissociation energy (BDE) [34]. Fig. 5 shows the rate coefficients of several relevant 1,2-insertion reactions of CH_2OO as a function of BDE. The rate coefficients of the title reactions are found to be close to the fitted red line. Further information on BDE and rate coefficients can be found in Table S13 in the Supporting Information.

Table 2 provides the rate coefficients for SCIs reactions with ammonia and various amines. It is observed that the presence of a methyl substitute on the amin increases its reactivity toward SCIs. For instance, the reaction between CH_2OO and methylamine is approximately two orders of magnitude faster compared to that with ammonia [8,22,35]. Mull et al. have calculated that the reaction of anti-conformer of methyl Criegee Intermediate (*anti*-CH_3CHOO) with methylamine is

Table 1
Summary of experimental conditions and temperature-dependent rate coefficients for reactions between CH_2OO and $(C_2H_5)_2NH/C_2H_5NH_2$ at 283–328 K.

T/K	$[CH_2OO]_0/10^{12}$ cm^{-3}	$[(C_2H_5)_2NH]/10^{13}$ cm^{-3}	$k_{4a}/10^{-11}$ cm^3 molecule^{-1} s^{-1}	$[CH_2OO]_0/10^{12}$ cm^{-3}	$[C_2H_5NH_2]/10^{13}$ cm^{-3}	$k_{4b}/10^{-12}$ cm^3 molecule^{-1} s^{-1}
283	5.14	2.13–11.50	**2.89 ± 0.45**	4.88	2.19–12.84	**9.21 ± 1.41**
298	5.14	2.17–11.55	**2.49 ± 0.39**	4.88	2.14–12.85	**8.14 ± 1.25**
308	5.14	2.16–11.57	**2.23 ± 0.35**	4.88	2.22–13.31	**7.59 ± 1.16**
318	5.14	2.16–11.58	**1.96 ± 0.31**	4.95	2.21–13.09	**7.10 ± 1.09**
328	5.14	2.15–11.48	**1.78 ± 0.28**	4.95	2.16–12.71	**6.60 ± 1.01**

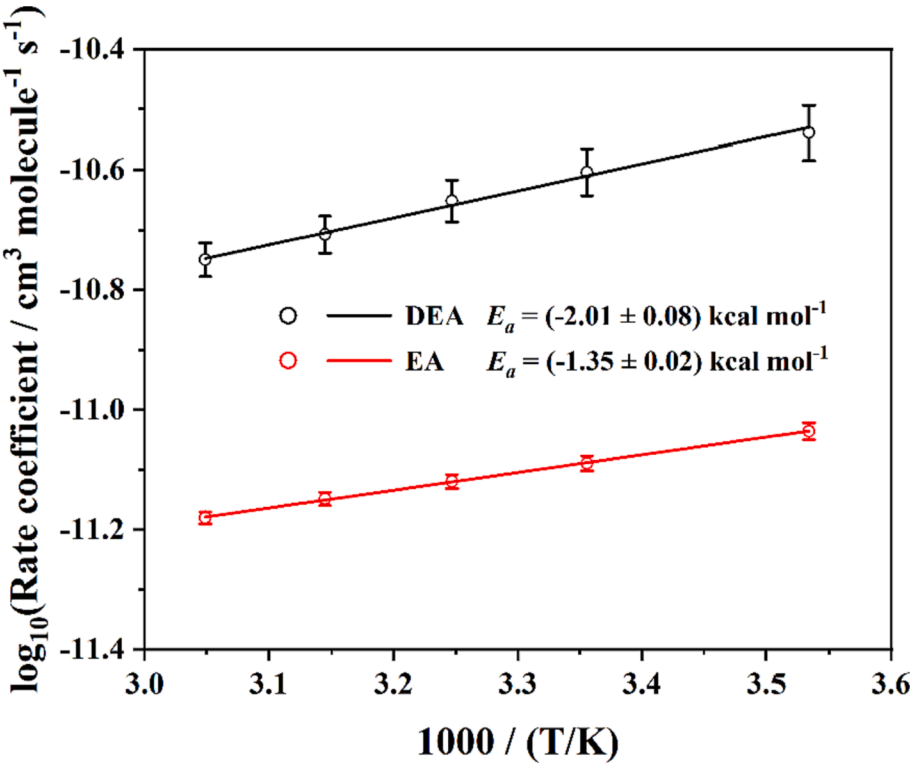

Fig. 4. Temperature-dependent rate coefficients (hollow dots) and the fits (red solid lines) using Arrhenius equation. The error bar represents the total experimental errors. (For interpretation of the references to colour in this figure legend, the reader is referred to the web version of this article.)

slightly faster than that of CH_2OO [36]. The reactivity between amines and SCIs is highly dependent on the conformer. For example, the reactions of *anti*-CH_3CHOO with MA and DMA are approximately four orders of magnitude faster than the corresponding reactions of *syn*-CH_3CHOO. Despite the lower concentrations of amines in the atmosphere (approximately 14–23 % of ammonia mass [14]), their reactivity towards CH_2OO is two to three orders of magnitude higher than that of ammonia. Considering these factors, the consumption of CH_2OO by amines is more significant than that by ammonia and may even compete with water under certain conditions.

3.2. Atmospheric impacts

Amines are involved in acid-base reactions with inorganic or organic acids in clouds, fog, or water microdroplets, leading to the new particle formation (NPF) [15,18]. Measurements have shown the presence of low molecular weight alkylamines in various environments. For instance, Rural areas in the United States have recorded DEA concentration of approximately 0.15 ppbv [37,38]. In the delta region of China, measurements have revealed varying concentrations of four amines (MA, DMA, DEA, TMA), with DEA exhibiting the highest concentration (6.83×10^{-3}–10.08×10^{-3} ppbv) [39]. In an industrial dairy located in Northern California, DEA concentrations were reported to be as high as 63.86–77.46 ppbv [40]. Furthermore, Amines exhibit seasonal variations, with DMA and EA concentrations peaking in winter [38], while DEA concentration reaches its highest level in summer [41].

In the troposphere, the primary atmospheric degradation pathway for amines is their reaction with OH radicals. The estimated lifetime of EA is 10–11.7 h, while that of DEA is 2.3–3.4 h [38]. Considering typical atmospheric concentrations of SCIs and OH, which range from $10^4 \sim 10^5$ [42,43] and $10^4 \sim 10^6$ molecules cm^{-3} [44], respectively, and the fact that the rate coefficient of the OH reaction is approximately five times faster than that of CH_2OO, the consumption of DEA by CH_2OO is relatively minor compared to that by OH, as shown in Figs. S5 and S6, and Tables S14 and S15 in the Supporting Information.

In indoor environments, ozone, a prevalent indoor oxidant [45], can react with alkenes that are commonly found indoors, originating from sources such as air fresheners, skin oil, and cleaning events [46,47], leading to the formation of SCIs. In these indoor environments, where light levels are typically three orders of magnitude lower than outdoors [48], the concentration of OH may drop significantly. As a result, reactions involving CH_2OO may play a role in the consumption of DEA and EA, sources of which include outdoor-to-indoor transport, smoking, cooking, and humidifiers [49].

Previous studies have shown that atmospheric CH_2OO is primarily consumed by water vapor and formic acid [13]. From Figs. S7 and S8, and Table S16 in the Supporting Information, it is evident that at room temperature, CH_2OO is primarily consumed by water vapor, even at relatively low humidity levels such as 20 %. As the temperature decreases, the reaction of CH_2OO with formic acid becomes dominant, and

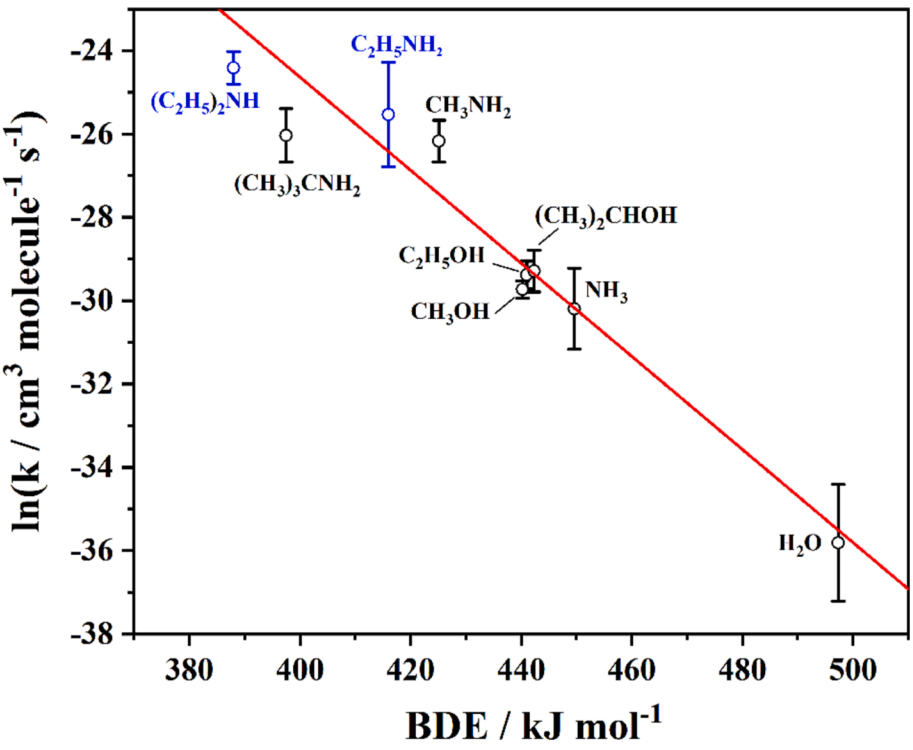

Fig. 5. Rate coefficients for several 1,2-insertion reactions of CH_2OO as a function of BDE. The blue points are the result of the current work. The circle are the experimental data points, and the red line is the linear fit. (For interpretation of the references to colour in this figure legend, the reader is referred to the web version of this article.)

Table 2
Summary of the reaction rate coefficients of CI and amines.

Reaction	k (cm^3 s^{-1})	Conditions (P, T)	Method	References
$CH_2OO + NH_3$	$(8.4 \pm 1.2) \times 10^{-14}$	10–100 Torr, 293 K	Cavity ring-down spectroscopy	Chhantyal-Pun et al. [8]
	$(6.7 \pm 0.7) \times 10^{-14}$	100–766 Torr, 298 K	UV absorption	Chao et al. [35]
	$(5.64 \pm 0.56) \times 10^{-14}$	50 Torr, 298 K	OH LIF	Liu et al. [22]
$CH_2OO + CH_3NH_2$	$(5.6 \pm 0.4) \times 10^{-12}$	10–100 Torr, 293 K	Cavity ring-down spectroscopy	Chhantyal-Pun et al. [8]
	8.88×10^{-12}	298 K	Theoretical	Mull et al. [36]
syn-$CH_3CHOO + CH_3NH_2$	2.4×10^{-15}	298 K	Theoretical	Vansco et al. [25]
	5.03×10^{-15}	298 K	Theoretical	Mull et al. [36]
anti-$CH_3CHOO + CH_3NH_2$	1.97×10^{-11}	298 K	Theoretical	Mull et al. [36]
syn-CH_3CHOO+ $(CH_3)_2NH$	2.4×10^{-14}	298 K	Theoretical	Vansco et al. [25]
anti-CH_3CHOO+$(CH_3)_2NH$	8.0×10^{-10}	298 K	Theoretical	Vansco et al. [25]
CH_2OO+$(CH_3)_3CNH_2$	$(4.95 \pm 0.64) \times 10^{-12}$	5–75 Torr, 298 K	OH LIF	Chen et al. [24]
CH_2OO+$(C_2H_5)_2NH$	$(2.49 \pm 0.39) \times 10^{-11}$	5.4–75 Torr, 298 K	OH LIF	This work
$CH_2OO + C_2H_5NH_2$	$(8.14 \pm 1.25) \times 10^{-12}$	5.4–75 Torr, 298 K	OH LIF	This work

the contribution of DEA to the consumption of CH_2OO increases.

4. Conclusion

In this study, we have determined the bimolecular rate coefficients of CH_2OO reactions with diethylamine (DEA) and ethylamine (EA) using the OH LIF method. Notably, both reactions exhibit significant negative temperature dependence. The rate coefficients for the CH_2OO reaction with DEA are (2.89 ± 0.45), (2.49 ± 0.39), (2.23 ± 0.35), (1.96 ± 0.31), and $(1.78 \pm 0.28) \times 10^{-11}$ cm^{-3} molecules s^{-1} at 10 Torr, while for the CH_2OO reaction with EA, they are (9.21 ± 1.41), (8.14 ± 1.25), (7.59 ± 1.16), (7.10 ± 1.09), and $(6.60 \pm 1.01) \times 10^{-12}$ cm^{-3} molecules s^{-1} at 30 Torr, measured at 283, 298, 308, 318, and 328 K, respectively. We did not observe any pressure dependence within the range of 5.4–75 Torr. Our findings suggest that at low temperatures, DEA and EA can surpass water vapor in the consumption of CH_2OO. Furthermore, under certain conditions where the concentration of DEA and EA are high, they may play a noticeable role in the consumption of CH_2OO.

CRediT authorship contribution statement

Jiayu Shi: Conceptualization, Data curation, Formal analysis, Methodology, Writing – original draft. **Haotian Jiang:** Conceptualization, Data curation, Methodology. **Li Che:** Conceptualization, Methodology, Supervision, Visualization, Resources, Writing – review & editing. **Siyue Liu:** Data curation, Methodology. **Yang Chen:** Data curation, Methodology. **Xueming Yang:** Project administration, Supervision, Resources, Visualization. **Wenrui Dong:** Conceptualization, Funding acquisition, Methodology, Project administration, Supervision, Validation, Visualization, Resources, Writing – review & editing.

Declaration of Competing Interest

The authors declare that they have no known competing financial interests or personal relationships that could have appeared to influence the work reported in this paper.

Data availability

Data will be made available on request.

Acknowledgements

The authors gratefully acknowledge the Dalian Coherent Light Source (DCLS) for support and assistance. This work was funded by the National Natural Science Foundation of China (NSFC No. 22288201, 21973010), Chinese Academy of Sciences (GJJSTD20220001), and Innovation Program for Quantum Science and Technology (No. 2021ZD0303305), L. Che thanks the Liaoning Revitalization Talents Program (Grant No. XLYC1907032).

Appendix A. Supplementary data

Supplementary data to this article can be found online at https://doi.org/10.1016/j.cplett.2023.140885.

References

[1] D.E. Heard, Annu. Rev. Phys. Chem. 57 (2006) 191.
[2] R. Criegee, Angew. Chem. Int. Ed. Eng. 14 (1975) 745.
[3] R. Criegee, G. Wenner, Justus Liebigs Ann. Chem. 564 (1949) 9.
[4] C.A. Taatjes, D.E. Shallcross, C.J. Percival, PCCP 16 (2014) 1704.
[5] L. Vereecken, J.S. Francisco, Chem. Soc. Rev. 41 (2012) 6259.
[6] L. Vereecken, A. Novelli, D. Taraborrelli, PCCP 19 (2017) 31599.
[7] A. Novelli, L. Vereecken, J. Lelieveld, H. Harder, PCCP 16 (2014) 19941.
[8] R. Chhantyal-Pun, R.J. Shannon, D.P. Tew, R.L. Caravan, M. Duchi, C. Wong, A. Ingham, C. Feldman, M.R. McGillen, M.A.H. Khan, I.O. Antonov, B. Rotavera, K. Ramasesha, D.L. Osborn, C.A. Taatjes, C.J. Percival, D.E. Shallcross, A.J. Orr-Ewing, PCCP 21 (2019) 14042.
[9] L. Onel, R. Lade, J. Mortiboy, M.A. Blitz, P.W. Seakins, D.E. Heard, D. Stone, PCCP 23 (2021) 19415.
[10] C. Cabezas, Y. Endo, PCCP 22 (2020) 446.
[11] R.A. Cox, Chem. Soc. Rev. 41 (2012) 6231.
[12] J.N. Yang, K. Takahashi, J.J. Lin, Chem. A Eur. J. 126 (2022) 6160.
[13] R.A. Cox, M. Ammann, J.N. Crowley, H. Herrmann, M.E. Jenkin, V.F. McNeill, A. Mellouki, J. Troe, T.J. Wallington, Atmos. Chem. Phys. 20 (2020) 13497.
[14] A. Sorooshian, S. Murphy, S. Hersey, H. Gates, L. Padro, A. Nenes, F. Brechtel, H. Jonsson, R. Flagan, J. Seinfeld, Atmos. Chem. Phys. 8 (2008) 5489.
[15] J. Almeida, S. Schobesberger, A. Kürten, I.K. Ortega, O. Kupiainen-Määttä, A. P. Praplan, A. Adamov, A. Amorim, F. Bianchi, M. Breitenlechner, Nature 502 (2013) 359.
[16] T. Kurten, V. Loukonen, H. Vehkamäki, M. Kulmala, Atmos. Chem. Phys. 8 (2008) 4095.
[17] H. Yu, R. McGraw, S.H. Lee, Geophys. Res. Lett. 39 (2012) L02807.
[18] J.N. Smith, K.C. Barsanti, H.R. Friedli, M. Ehn, M. Kulmala, D.R. Collins, J.H. Scheckman, B.J. Williams, P.H. McMurry, Proceedings of the National Academy of Sciences 107 (2010) 6634.
[19] S. Li, K. Qu, H. Zhao, L. Ding, L. Du, Chem. Phys. 472 (2016) 198.
[20] T. Bergman, A. Laaksonen, H. Korhonen, J. Malila, E.M. Dunne, T. Mielonen, K.E. J. Lehtinen, T. Kühn, A. Arola, H. Kokkola, J. Geophys. Res. Atmos. 120 (2015) 9606.
[21] F. Ma, H.B. Xie, R. Zhang, L. Su, Q. Jiang, W. Tang, J. Chen, M. Engsvang, J. Elm, X. C. He, Environ. Sci. Tech. 57 (2023) 6944.
[22] Y. Liu, C. Yin, M.C. Smith, S. Liu, M. Chen, X. Zhou, C. Xiao, D. Dai, J.J. Lin, K. Takahashi, W. Dong, X. Yang, PCCP 20 (2018) 29669.
[23] M. Kumar, J.S. Francisco, Chem. Sci. 10 (2019) 743.
[24] Y. Chen, H. Jiang, S. Liu, J. Shi, Y. Jin, X. Yang, W. Dong, Chem. A Eur. J. 127 (2023) 2432.
[25] M.F. Vansco, M. Zou, I.O. Antonov, K. Ramasesha, B. Rotavera, D.L. Osborn, Y. Georgievskii, C.J. Percival, S.J. Klippenstein, C.A. Taatjes, M.I. Lester, R. L. Caravan, Chem. A Eur. J. 126 (2022) 710.
[26] Y. Liu, F. Liu, S. Liu, D. Dai, W. Dong, X. Yang, PCCP 19 (2017) 20786.
[27] X. Zhou, Y. Chen, Y. Liu, X. Li, W. Dong, X. Yang, PCCP 23 (2021) 13276.
[28] Y. Liu, K.D. Bayes, S.P. Sander, Chem. A Eur. J. 118 (2014) 741.
[29] D. Stone, K. Au, S. Sime, D.J. Medeiros, M. Blitz, P.W. Seakins, Z. Decker, L. Sheps, PCCP 20 (2018) 24940.
[30] W.L. Ting, C.H. Chang, Y.F. Lee, H. Matsui, Y.P. Lee, J.J. Lin, J. Chem. Phys. 141 (2014), 104308.
[31] J.C. Mossinger, D.E. Shallcross, R.A. Cox, J. Chem. Soc. Faraday Trans. (1998) 1391.
[32] J.P. Misiewicz, S.N. Elliott, K.B. Moore, H.F. Schaefer, PCCP 20 (2018) 7479.
[33] L. Vereecken, H. Harder, A. Novelli, PCCP 14 (2012) 14682.
[34] R. Chhantyal-Pun, M.A.H. Khan, C.A. Taatjes, C.J. Percival, A.J. Orr-Ewing, D. E. Shallcross, Int. Rev. Phys. Chem. 39 (2020) 385.
[35] W. Chao, C. Yin, K. Takahashi, PCCP 21 (2019) 22589.
[36] H.F. Mull, G.J.R. Aroeira, J.M. Turney, H.F. Schaefer, PCCP 22 (2020) 22555.
[37] N.A. Freshour, K.K. Carlson, Y.A. Melka, S. Hinz, B. Panta, D.R. Hanson, Atmos. Meas. Tech. 7 (2014) 3611.
[38] E. Tzitzikalaki, N. Kalivitis, M. Kanakidou, Atmos. 12 (2021) 1454.
[39] W. Du, X. Wang, F. Yang, K. Bai, C. Wu, S. Liu, F. Wang, S. Lv, Y. Chen, J. Wang, AdAtS 38 (2021) 1128.
[40] N.E. Rabaud, S.E. Ebeler, L.L. Ashbaugh, R.G. Flocchini, Atmos. Environ. 37 (2003) 933.
[41] A.-J. Kieloaho, H. Hellén, H. Hakola, H.E. Manninen, T. Nieminen, M. Kulmala, M. Pihlatie, Atmos. Environ. 80 (2013) 369.
[42] A. Novelli, K. Hens, C. Tatum Ernest, M. Martinez, A.C. Nölscher, V. Sinha, P. Paasonen, T. Petäjä, M. Sipilä, T. Elste, C. Plass-Dülmer, G.J. Phillips, D. Kubistin, J. Williams, L. Vereecken, J. Lelieveld, H. Harder, Atmos. Chem. Phys. 17 (2017) 7807.
[43] M.A.H. Khan, C.J. Percival, R.L. Caravan, C.A. Taatjes, D.E. Shallcross, Environ Sci Process Impacts 20 (2018) 437.
[44] D. Stone, L.K. Whalley, D.E. Heard, Chem. Soc. Rev. 41 (2012) 6348.
[45] C.J. Weschler, Indoor Air 10 (2000) 269.
[46] B.L. Deming, P.J. Ziemann, Indoor Air 30 (2020) 914.
[47] D.E. Shallcross, C.A. Taatjes, C.J. Percival, Indoor Air 24 (2014) 495.
[48] W. Nazaroff, C. Weschler, R. Corsi, Atmospheric Environ. 37 (2003) 5451.
[49] W.W. Nazaroff, C.J. Weschler, Indoor Air 30 (2020) 559.